ACSNANO

www.acsnano.org

ARTICLE

Identification of Single-Molecule Catecholamine Enantiomers Using a Programmable Nanopore

Wendong Jia, Chengzhen Hu, Yuqin Wang, Yao Liu, Liying Wang, Shanyu Zhang, Qiang Zhu, Yuming Gu, Panke Zhang, Jing Ma, Hong-Yuan Chen, and Shuo Huang*

Cite This: https://doi.org/10.1021/acsnano.2c01017

ABSTRACT: Enantiomers, chiral isomers with opposite chirality, typically demonstrate differences in their pharmacological activity, metabolism, and toxicity. However, direct discrimination between enantiomers is challenging due to their similar physiochemical properties. Following the strategy of programmable nanoreactors for stochastic sensing (PNRSS), introduction of phenylboronic acid (PBA) to a *Mycobacterium smegmatis* porin A (MspA) assists in the identification of the enantiomers of norepinephrine and epinephrine. Using a machine learning algorithm, identification of the enantiomers has been achieved with an accuracy of 98.2%. The enantiomeric excess (ee) of a mixture of enantiomeric catecholamines was measured to determine the enantiomeric purity. This sensing strategy is a faster method for the determination of ee values than liquid chromatography−mass spectrometry and is useful as a quality control in the industrial production of enantiomeric drugs.

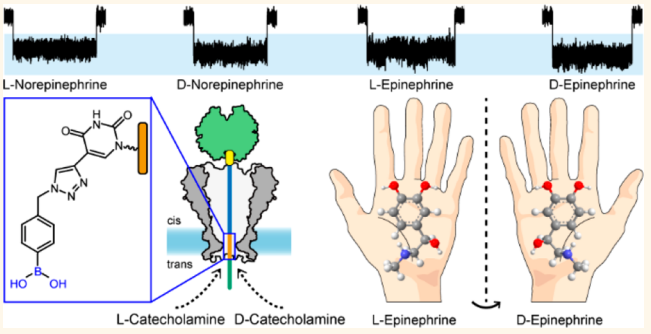

KEYWORDS: *chirality, catecholamine enantiomer, programmable nanoreactors, Mycobacterium smegmatis porin A, single-molecule chemistry*

INTRODUCTION

Many biologically significant molecules, including amino acids, nucleotides, and saccharides, are chiral in nature.[1,2] Enantiomers, which are chiral isomers with opposite chirality,[3] usually demonstrate differences in their pharmacology, metabolism, and toxicity and have the same chemical composition and very similar physiochemical properties.[4−7] Accordingly, direct discrimination between them is difficult. Catecholamines (CA) such as norepinephrine, epinephrine, and dopamine are important neurotransmitters and hormones that play critical roles in vasoconstriction, blood pressure control, and the transmission of nerve impulses.[8] Both norepinephrine and epinephrine are used as emergency medicines in cardiac arrest and anaphylaxis.[9,10] Both norepinephrine and epinephrine contain a single chiral center, and each have two enantiomers with different pharmacodynamic effects.[11] For example, the activity in vivo of the corresponding L-enantiomers is 100 times that of the D-enantiomers.[12] In the production of L-norepinephrine (L-N) and L-epinephrine (L-E), D-norepinephrine (D-N) and D-epinephrine (D-E) are generally treated as undesired products which affect the synthesis efficiency and product quality.[13−17] The L-enantiomers are spontaneously converted into D-enantiomers by racemization, and this results in gradual loss of their therapeutic effectiveness, posing challenges to drug storage.[18] Therefore, for the quality control of pharmaceutical production, it is necessary to develop a rapid enantiomer identification method for norepinephrine and epinephrine. Conventionally, detection of catecholamine enantiomers is carried out by high-performance liquid chromatography (HPLC) using chiral-specific columns[19] with or without derivatization of the catecholamine enantiomers prior to the HPLC analysis.[20] Chiral-specific detectors, such as circular dichroism (CD)[21] or optical rotation,[22] are used for enantiomer detection, but these methods depend on reliable separation methods.

Biological nanopores[23] are a group of transmembrane porin-based sensors originally developed for sequencing of single

Received: January 29, 2022
Accepted: April 5, 2022

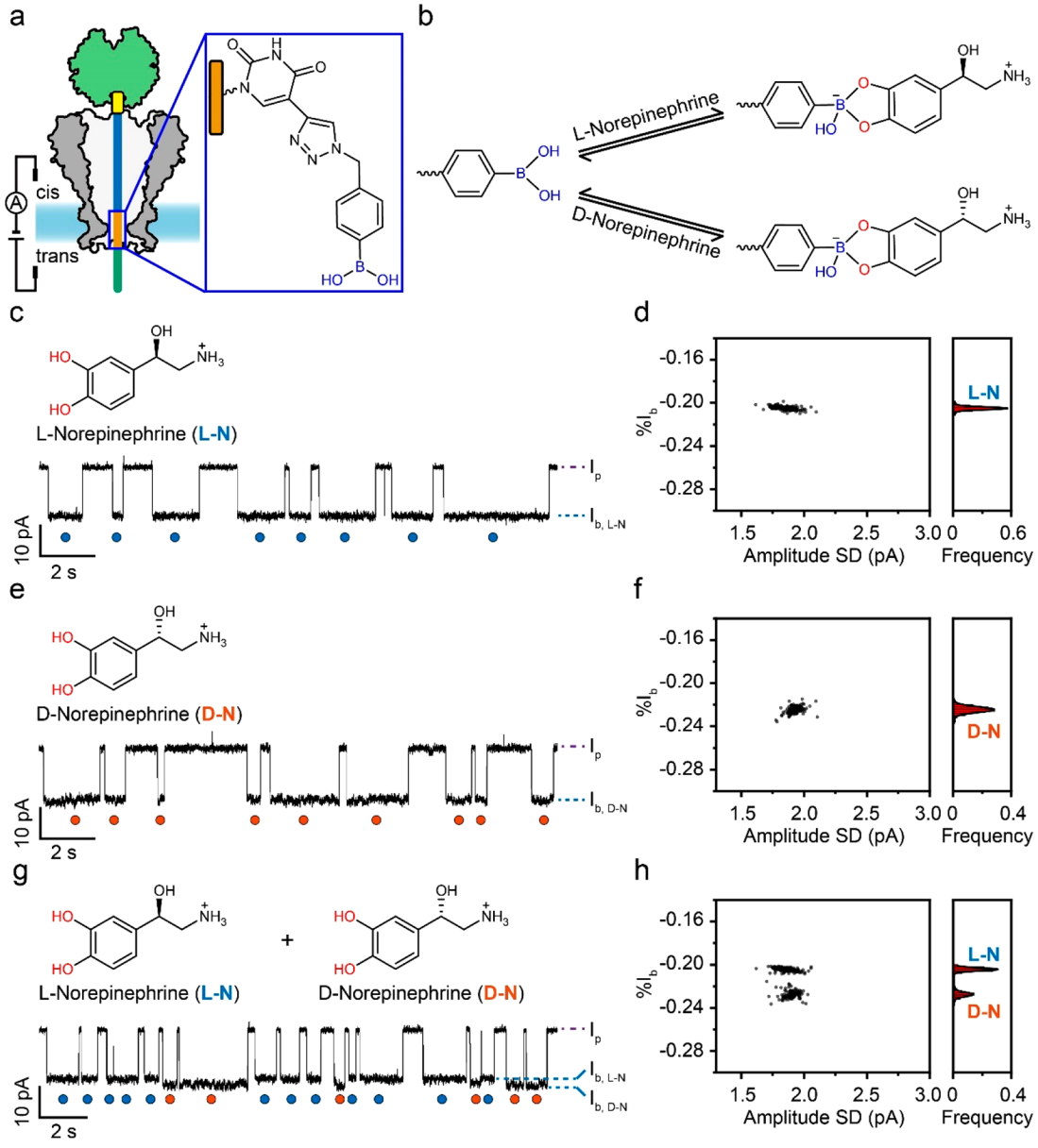

Figure 1. Discrimination of norepinephrine enantiomers using PNRSS. (a) Schematic diagram. The MspA serves to dock a streptavidin-tethered PNRSS strand (14PBA, Supplementary Table 1). The reaction section (brown), which is located at the pore restriction, contains a phenylboronic acid (PBA). The PBA serves as the fixed reactant, capable of binding mobile reactants such as catecholamines to report sensing events. The blue, green, and yellow regions, respectively, represent the extension section, the traction section, and the tether site of a PNRSS strand. (b) Mechanism of L-norepinephrine (L-N) or D-norepinephrine (D-N) binding to a PBA. (c–h) Results acquired when samples containing different combinations of L-norepinephrine and D-norepinephrine are added to the device. The corresponding event scatter plots and histograms (d,f,h) are placed to the right of each corresponding trace (c,e,g). Catecholamines were added to *trans* with a final concentration of 200 μM. (g) Representative trace acquired when L- and D-norepinephrine are simultaneously added to *trans*, each with a 100 μM final concentration. (h) Corresponding event scatter plot. The measurements were carried out as described in Methods. A buffer of 1.5 M KCl, 10 mM HEPES, pH 8.0 was used. A +140 mV potential voltage was continually applied. For demonstration purposes, the traces presented in c, e, and g were low-pass filtered by a Bessel filter with a cutoff frequency of 100 Hz. In all representative traces, characteristic events of L- and D-norepinephrine are marked, respectively, with blue and orange circles. The corresponding histogram of $\%I_b$, superimposed with its Gaussian fitting result, is plotted to the right of each scatter plot in d, f, and h. Events in the scatter plots from 10 min are continually recorded trace in each condition: 184 (d), 147 (f), and 308 (h) events are included in the corresponding scatter plot.

molecules. Their high sensing resolution also enables direct probing of metal ions,[24] small molecules,[25] nucleic acids,[26] peptides,[27] and proteins[28] at the level of a single molecule. With their chiral lumen environment and a sufficient resolution of sensing, biological nanopores can, in principle, discriminate between enantiomers when the target molecule is transiently trapped near the pore constriction. However, owing to the technical complexity associated with the chemical engineering of the pore lumen, direct discrimination of enantiomers has been only rarely reported with nanopores.[29−32] Programmable nanoreactors for stochastic sensing (PNRSS)[33] is a versatile, recently developed strategy to probe single-molecule reactions. It omits the complexities associated with pore engineering by introducing instead a synthetic strand of chemically engineered

https://doi.org/10.1021/acsnano.2c01017
ACS Nano XXXX, XXX, XXX−XXX

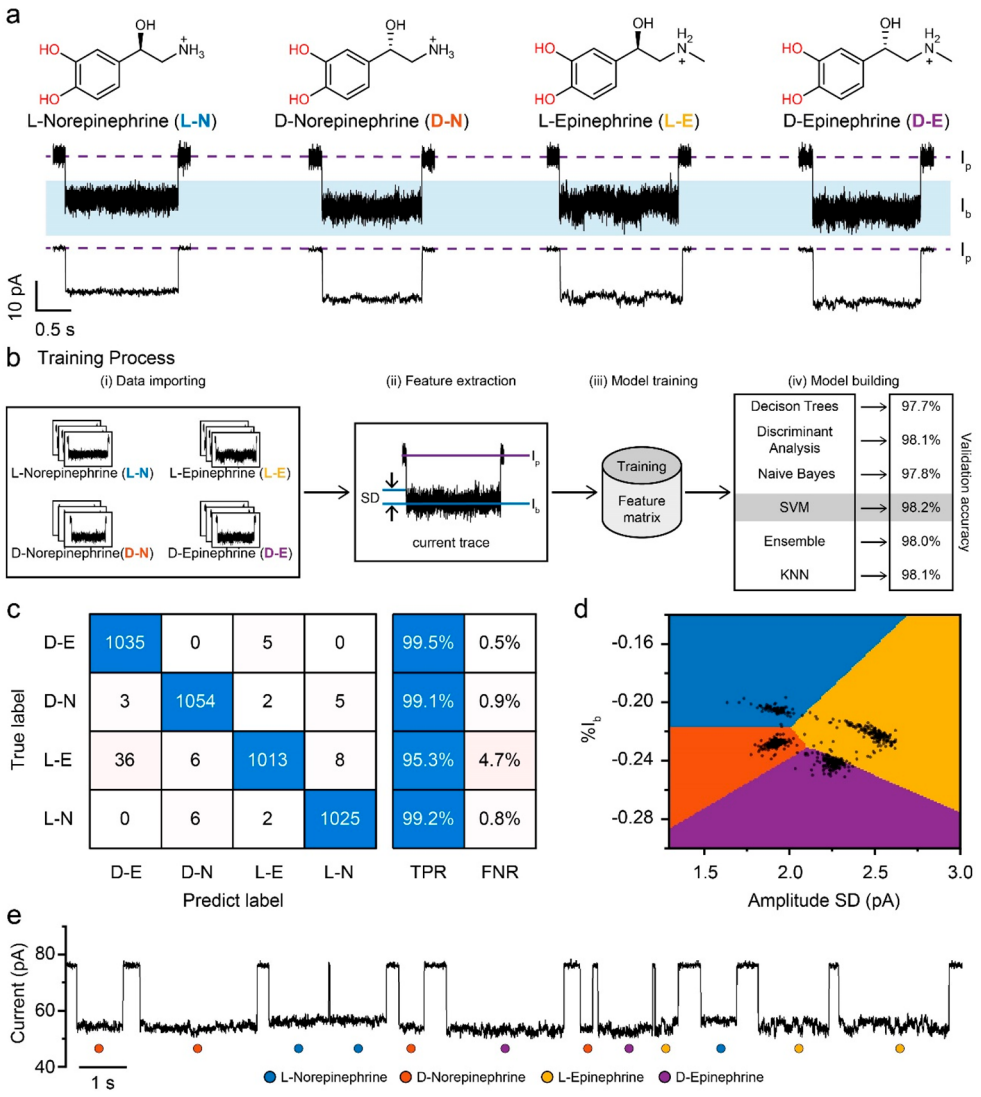

Figure 2. Identification of norepinephrine and epinephrine enantiomers assisted by machine learning. (a) Chemical structures (top) of L-norepinephrine (L-N), D-norepinephrine (D-N), L-epinephrine (L-E), and D-epinephrine (D-E) and their corresponding nanopore events (middle and bottom). Nanopore events presented in the bottom were low-pass filtered at 100 Hz. (b) Flow diagram of the training process. Four classes of events, including L-norepinephrine, D-norepinephrine, L-epinephrine, and D-epinephrine events, were collected to form the input data set. The amplitude SD and percentage blockade $\%I_b$ of all events were extracted to form a data table also referred to as a feature matrix. Each row of the feature matrix represents a binding event, including two feature parameters, SD and $\%I_b$. Features from 4200 events were fed into models in the Classification Learner Toolbox of MATLAB for model training. A 10-fold cross-validation was performed, and their cross-validation accuracy scores were reported. Among the models being tested, the linear SVM model reported the highest accuracy score of 98.2% and the lowest total misclassification cost. (c) The confusion matrix result produced by the linear support vector machine model. True positive rate and false negative rate were also demonstrated to the right. (d) Scatter plot of amplitude SD versus percentage blockade $\%I_b$. The results are based on 613 events acquired with a mixture of four catecholamines. The decision boundary, which separates the scatter plot into blue (L-N), orange (D-N), yellow (L-E), and purple (D-E) regions, was determined from the machine learning results. (e) Representative trace containing events of four catecholamine enantiomers. The trace was low-pass filtered at 100 Hz by a Bessel filter. Characteristic events were recognized by the machine learning algorithm and labeled on the trace. All nanopore measurements were performed as described in Methods. Each catecholamine was added to *trans* with a concentration of 200 μM.

nucleic acid strands to the pore lumen. To the best of our knowledge, sensing of enantiomers by PNRSS has not been reported to date. Here, it is used to discriminate between catecholamine enantiomers, including L-norepinephrine, D-norepinephrine, L-epinephrine, and D-epinephrine. PNRSS does not require chemical separation of enantiomers, and enantiomeric excess (ee) values can be determined in less than 10 min. The amount of sample required for a single measurement is 0.5 nmol, which is much less than is required for HPLC.[33] Assisted with a custom machine learning algorithm, a 98.2% accuracy has been achieved.

RESULTS AND DISCUSSION

Discrimination between Catecholamine Enantiomers Using PNRSS. Both norepinephrine and epinephrine are catecholamines. They both contain a *cis*-diol moiety and differ in the substituent on the nitrogen atom. Phenylboronic acid (PBA) can reversibly form cyclic boronates with *cis*-diols, and this mechanism has been widely used to construct sensors and

https://doi.org/10.1021/acsnano.2c01017
ACS Nano XXXX, XXX, XXX−XXX

separation systems for polyols.[34] PBA can be introduced into the lumen of MspA following a PNRSS strategy (Figure 1a,b). First, the PNRSS strand 14TAK (Supplementary Table 1) was reacted with 4-(azidomethyl)benzeneboronic acid by Huisgen copper-(I)-catalyzed azide−alkyne 1,3-dipolar cycloaddition (CuAAC)[35] to generate 14PBA (Methods and Supplementary Table 1). The 14PBA produced in this way was further characterized by mass spectrometry and single channel recording, confirming the success of the reaction (Supplementary Figures 1 and 2). During the nanopore measurements (Methods), an octameric M2MspA nanopore was applied to dock the PNRSS strand electrophoretically. For simplicity, this MspA mutant is referred to hereafter as MspA. The mutations of the M2MspA in reference to its wild type were introduced to optimize the internal charge of the pore lumen,[36] so that translocation of DNA is permitted. To precisely locate the PBA to the pore constriction, the length of the extension section could be optimized with a 3.5 Å precision to reach an optimum location (Figure 1a).

Experimentally, two chambers filled with electrolyte buffer were separated by a self-assembled lipid membrane into which an MspA has been inserted. The electrically grounded chamber is defined as *cis*, and the opposing chamber is defined as *trans*. With a +140 mV potential continually applied, an unoccupied MspA nanopore reports an open pore current (I_0). When a streptavidin-tethered 14PBA was captured electrophoretically, the nanopore current immediately dropped to the static blockage current (I_p) (Supplementary Table 2). In order to achieve an optimal sensing performance, the PBA is designed to be close to the pore constriction when the 14PBA is fully stretched in the pore lumen (Figure 1a). Subsequently, with the addition of D-norepinephrine to *trans*, the nanopore current reached a further blockage level (I_b). Continuous switching between I_p and I_b corresponds to the switching between the state when the PBA is unbound or bound by a D-norepinephrine (Supplementary Figure 3). However, these events were not observed on 14TAK (Supplementary Table 1), again confirming that the PBA is critical in the generation of the events (Supplementary Figure 2a). The key parameters of PNRSS measurement, including the dwell time t_{off} and the interevent interval t_{on}, are defined in Supplementary Figure 3. The percentage blockade $\%I_b$ is derived from $(I_b - I_p)/I_p$. The amplitude standard deviation (SD) is used to evaluate the noise level of the events.

Then norepinephrine enantiomers were added to *trans* at a desired concentration, and the rate of event appearance increases at higher concentrations (Supplementary Figures 4 and 5). Although the events caused by binding of D- or L-norepinephrine have similar kinetic constants (Supplementary Table 4) and SD values, they can, however, be clearly distinguished by the difference in their percentage blockades, $\%I_b$. Specifically, the addition of L-norepinephrine reported an average $\%I_b$ of approximately −0.207 (Figure 1c,d). The addition of D-norepinephrine produced an average $\%I_b$ of approximately −0.229 (Figure 1e,f and Supplementary Table 3). Thus, events of D- and L-norepinephrine can be directly identified even if they are simultaneously sensed in a mixture (Figure 1g,h and Supplementary Figure 6).

Following the same principle, sensing of epinephrine enantiomers was also evaluated by PNRSS (Supplementary Figures 7−9). The average percentage blockade $\%I_b$ produced by L- and D-epinephrine is approximately −0.226 and −0.248, respectively (Supplementary Table 3). D-Epinephrine has an event amplitude larger than that of L-epinephrine. The noise levels of L- and D-epinephrine are also significantly different. The binding events caused by L-epinephrine have a highly characteristic noise signature and thus a larger SD (∼7% larger). The events associated with epinephrine enantiomers can be identified by considering their amplitude and SD features simultaneously (Supplementary Figure 9).

The event amplitude of all four types of catecholamines follows the order of D-E > L-E ≈ D-N > L-N. This is expected because epinephrine has an additional methyl group compared to norepinephrine, and this impedes more ionic current, producing a larger event amplitude. Although L-epinephrine (L-E) and D-norepinephrine (D-N) have similar event amplitudes, they were sufficiently distinguished by the SD of the event (Supplementary Figure 10). Specifically, the L-norepinephrine consistently reports a flat blockage level. Low-frequency level fluctuations were, however, frequently observed with other catecholamine enantiomers. Though the molecular nature of this phenomenon remains not fully understood, it is speculated that the fluctuation may correspond to reversible switching between different conformational states of the analyte when trapped in a nanoconfined space. A systematic study using molecular dynamics simulations may be carried out in a follow-up study to further explain this phenomenon. Experimentally, the above results confirm the discrimination between catecholamine enantiomers, carried out by a PNRSS assay.

Machine Learning Assisted Identification of Norepinephrine and Epinephrine Enantiomers. Machine learning, which learns from the input data without focusing on the programming, is a branch of artificial intelligence. It has been widely applied in nanopore research to automate event classification and to evaluate sensing performance.[33,37−39] The catecholamine sensing events produced by PNRSS report highly consistent event features for each type of analyte being tested (Figure 2a and Supplementary Figure 11), suggesting that these data are suitable for automatic identification with a custom machine learning algorithm.

The training process of the machine learning algorithm consists of four steps, as described in Figure 2b. Briefly, the characteristic events produced by L-norepinephrine, D-norepinephrine, L-epinephrine, and D-epinephrine formed the input data set. The events for each type of enantiomer were acquired separately with a single type of catecholamine added so that all produced events have known labels. A total of 4200 events were included. Events of epinephrine report a highly characteristic low-frequency fluctuation, producing large event SD values. The fluctuation frequency range for D- and L-epinephrine was 4.2 ± 1.5 and 2.9 ± 1.4 Hz, respectively. In order to avoid overlooking of this feature, only events with more than 200 ms of dwell time were included in the data set. Two event features, including amplitude SD and percentage blockade $\%I_b$, were extracted from characteristic events to form a feature matrix (Supplementary Figure 12). The selection of these two event features are based on the most obvious difference in the event characteristics (Figure 2a). The feature matrix was then fed into the Classification Learner toolbox of MATLAB for model training. Mainstream models, including decision trees, discriminant analysis, naive Bayes, support vector machine (SVM), *k* nearest neighbor (KNN), and ensemble were all investigated to identify the best performing model. A 10-fold cross-validation was applied for each model. Specifically, the data set was divided stochastically into the training data set for model training and the validation data set for fine-tuning of model parameters and

https://doi.org/10.1021/acsnano.2c01017
ACS Nano XXXX, XXX, XXX−XXX

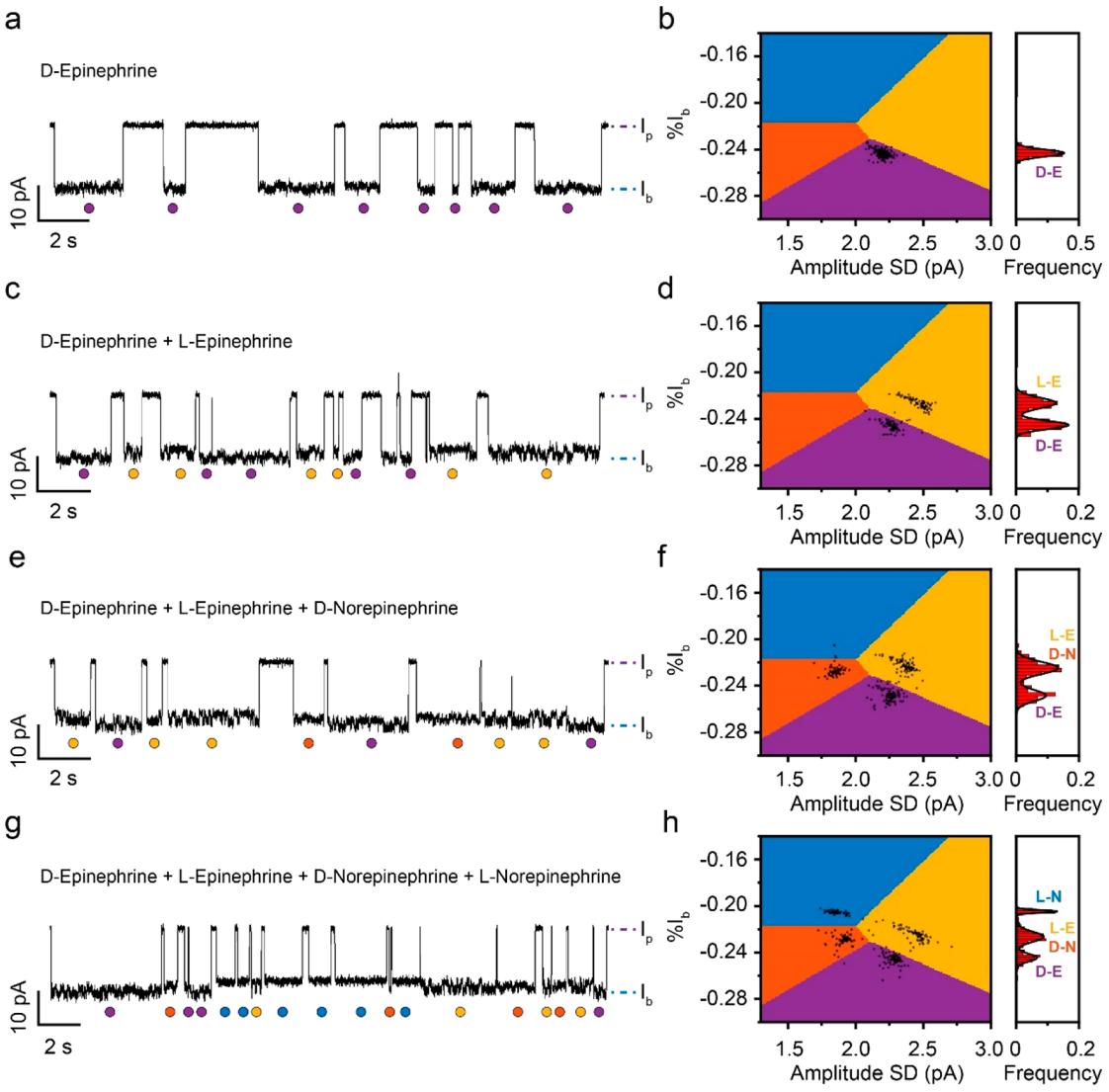

Figure 3. Sequential addition of D-epinephrine, L-epinephrine, D-norepinephrine, and L-norepinephrine. Representative traces were acquired when (a) D-epinephrine, (c) L-epinephrine, (e) D-norepinephrine, and (g) L-norepinephrine were sequentially added to *trans*. Events of D-epinephrine, L-epinephrine, D-norepinephrine, and L-norepinephrine were marked with purple, yellow, orange, and blue circles, respectively, on traces. b, d, f, and h, where the corresponding event scatter plot was generated from a 10 min trace acquired as described in a, c, e, and g. For demonstration purposes, the traces presented in a, c, e, and g were low-pass filtered by a Bessel filter with a cutoff frequency of 100 Hz. The decision boundary plot generated by the machine learning algorithm is placed on top of the scatter plot to assist the event recognition. Each addition of catecholamine enantiomers creates an extra distribution of events in the scatter plot. A buffer of 1.5 M KCl, 10 mM HEPES, pH 8.0 was used. A +140 mV potential was continuously applied. The concentration of each catecholamine enantiomer is 150 μM. A total of 143, 183, 250, and 275 events were included in the scatter plots of b, d, f, and h, respectively.

validation of the model. The linear SVM model has reported the highest accuracy of 98.2% and the lowest total misclassification cost. Here, the total misclassification cost represents the number of misclassified events in the selected model. The other model performances are summarized in Supplementary Table 7. The confusion matrix was generated based on the linear SVM model, from which the accuracy of L-norepinephrine, D-norepinephrine, L-epinephrine, and D-epinephrine identification was 99.2, 99.1, 95.3, and 99.5%, respectively (Figure 2c).

The linear SVM model was used to generate the decision boundary. A mesh grid was first generated within the region of 1.3−3.0 pA in the SD and −0.30 to −0.14 in the $\%I_b$ with intervals of 0.01 and 0.001, respectively (Figure 2d). The mesh grid contains the coordinates of the plane within the specified range, where the *x* and *y* coordinates, respectively, represent SD and $\%I_b$. Event type regions can be identified by these mesh grid parameters when inferred from the linear SVM model and colored blue (L-norepinephrine), orange (D-norepinephrine), yellow (L-epinephrine), and purple (D-epinephrine) so that the decision boundary is generated. When all enantiomers of norepinephrine and epinephrine were simultaneously sensed, the characteristic events were extracted from a 15 min continuous recording, and the feature parameters of SD and $\%I_b$ were obtained. The decision boundary generated by the machine learning algorithm was placed above the scatter plot of the mixture to assist event recognition. Each characteristic event in the recording with the mixture can be efficiently identified and labeled using this decision boundary (Figure 2e).

The trained model was then employed to predict unidentified events. The PNRSS measurement was carried out by sequential

https://doi.org/10.1021/acsnano.2c01017
ACS Nano XXXX, XXX, XXX−XXX

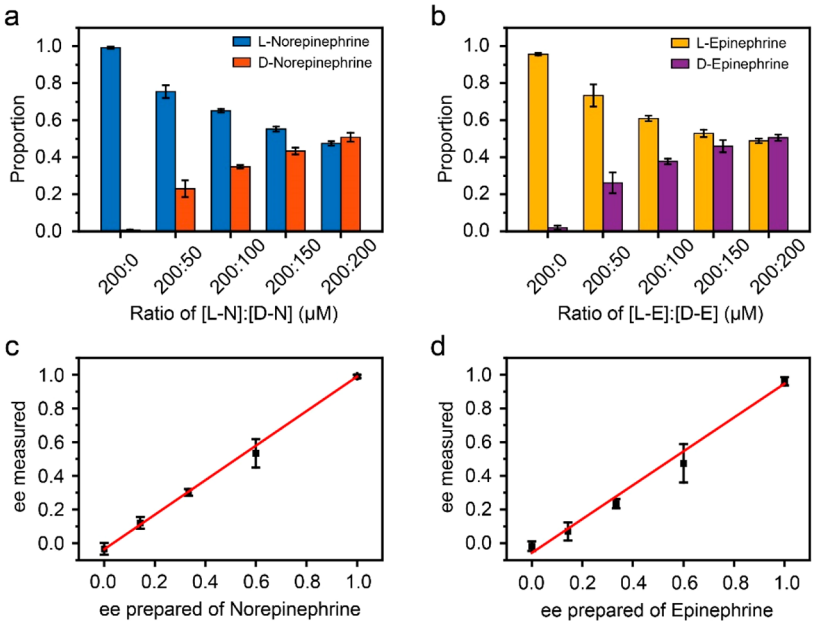

Figure 4. Detection of the enantiomeric purity in a mixture of catecholamine enantiomers. Event proportion histograms of (a) norepinephrine or (b) epinephrine enantiomers. The event proportion results were acquired by titrating D-catecholamine in 50 μM increments into a 200 μM L-catecholamine sample. The characteristic events were extracted from a 10 min continually recorded trace and identified by the machine learning algorithm to derive the event proportions. The relationship between the ee value of the prepared mixture of norepinephrine (c) or epinephrine (d) enantiomers and the ee measured by PNRSS. The fitting results report a slope of 1.02 ± 0.01 and the R^2 of 0.999 for (c) and a slope of 1.00 ± 0.05 and the R^2 of 0.991 for (d). A buffer of 1.5 M KCl, 10 mM HEPES, pH 8.0 was used. A +140 mV potential was continuously applied. Three independent measurements (N = 3) were performed for each condition to produce the statistics.

addition of D-epinephrine, L-epinephrine, D-norepinephrine, and L-norepinephrine to the same nanopore device (Figure 3a,c,e,g). A 10 min trace was recorded for each condition, and the event features were extracted. Four event populations, respectively, corresponding to binding of D-epinephrine, L-epinephrine, D-norepinephrine, and L-norepinephrine were clearly observed in the scatter plot (Figure 3b,d,f,h). This again demonstrates that this single-molecule assay can effectively discriminate between catecholamine enantiomers even if they are sensed simultaneously in a mixture. The machine learning algorithm, however, improves the efficiency of event classification, and no interference of human judgment is included.

Detection of Enantiomeric Purity. Enantiomeric excess value is a measure of the enantiomeric purity of a chiral material.[40] The determination of the enantiomeric purity is critical for the production and storage of norepinephrine and epinephrine medicinal products. As described above, the information provided by the nanopore readouts are sufficient to determine the value of the enantiomeric excess. Experimentally, D-norepinephrine was added to 200 μM L-norepinephrine in 50 μM increments to obtain a mixture of L- and D-norepinephrine at five different concentration ratios (Supplementary Figure 13) to produce nanopore readouts. The setting of the 50 μM concentration increments is intended to generate different ratios of D- and L-enantiomers in a mixture so that different ee values are measured and a general calibration curve is generated by fitting. For each condition, events from 10 min continuous recordings were extracted to form the predicting data sets, which were subsequently identified by the previously established machine learning model. The proportion of two enantiomers at each measurement was calculated. With the addition of D-norepinephrine, the event proportion of D-norepinephrine increased, while that of L-norepinephrine decreased, and ultimately, both events report similar proportions (Figure 4a). The same measurements were performed with epinephrine enantiomers, which gave similar results (Figure 4b and Supplementary Figure 14).

For the quantitative evaluation of ee determined with a PBA-modified programmable nanopore, calibration curves were generated from event proportions acquired in various known mixtures of L- and D-enantiomers (Figure 4c,d). The measured ee value is derived from $(P_L - P_D)/(P_L + P_D)$, where P represents the proportion of events caused by L- or D-enantiomers. The prepared ee value is obtained from the concentrations of L- and D-enantiomers by the formula: $([L] - [D])/([L] + [D])$. The slopes of 1.02 ± 0.01 and 1.00 ± 0.05 for norepinephrine and epinephrine were reported, signifying that the determined ee value from nanopore measurement is consistent with the expected value. The measured ee values, calculated from the event proportion of L- and D-catecholamines, were basically consistent with the prepared values, further demonstrating that the designed PNRSS assay can directly report the ee values for enantiomeric purity determination (Supplementary Tables 5 and 6).

To demonstrate an application of quality control for norepinephrine and epinephrine enantiomer medicine, the commercially supplied epinephrine hydrochloride injection was evaluated by the PNRSS sensor (Supplementary Figure 15). Experimentally, 15 μL of epinephrine hydrochloride injection sample was directly added to *trans*, and then corresponding binding events were immediately reported during the PNRSS measurement. The previously trained model was employed for event identification. The main component of epinephrine hydrochloride injection was confirmed to be L-epinephrine; however, residual D-epinephrine was still detected, and the ee value was derived to be 0.98. Though the demonstrated assay is

https://doi.org/10.1021/acsnano.2c01017
ACS Nano XXXX, XXX, XXX−XXX

simple, it clearly presents how PNRSS would be applied during a real application of medicine quality control. The sample is directly added, and no sample treatment is, however, required.

Acknowledging the high chemical selectivity of PBA introduced to the PNRSS strand, the assay may as well be carried out in the presence of a physiological sample background without causing any interferences. To show that, identification of epinephrine enantiomers was performed with a real human urine background, and the enantiomer discrimination is well achieved without any interferences (Supplementary Figure 16). However, due to the large measurement volume and the small sensing area of an individual nanopore, the sensing efficiency in this configuration is currently limited to 1 μM, as demonstrated with D-epinephrine sensing in 10 min of continuous recording (Supplementary Figure 17). In future prospects, to deal with sensing of extremely low concentration samples, a parallel nanopore array similar to that demonstrated by the MinION sequencer may be applied. This, however, requires significant engineering efforts, and the cost of the device would be higher. However, for any sensing applications when the analyte presents with a sufficiently high concentration, the current configuration is sufficient.

Identification of epinephrine enantiomers was also performed with the α-hemolysin (α-HL) nanopore (Supplementary Figure 18). Experimentally, D- and L-epinephrine were sequentially added to *trans* to reach the desired concentrations. Corresponding events of epinephrine enantiomers were subsequently observed. However, the event amplitude reported by the α-HL nanopore was much smaller than that generated by MspA. More importantly, the events generated by the two chiral molecules of epinephrine were not clearly distinguishable, suggesting that the selection of the pore type, which determines the resolution of sensing, is crucial in the identification of catecholamine enantiomers by PNRSS.

CONCLUSIONS

We have demonstrated single-molecule discrimination of norepinephrine and epinephrine enantiomers with a programmable nanopore modified with a phenylboronic acid. The PBA, which was introduced into the pore lumen using a PNRSS strategy, reacts with the *cis*-diol moiety of different catecholamines and reports their identities. Acknowledging the high resolution provided by the conical lumen geometry of MspA, four types of catecholamines, including L-norepinephrine, D-norepinephrine, L-epinephrine, and D-epinephrine, can be fully distinguished. Though not investigated in this study, the molecular conformation of these enantiomers when confined in the pore lumen may be demonstrated using molecular dynamics simulation in future prospects. Assisted by machine learning, the general accuracy score of catecholamine enantiomer identification was 98.2%, and events from a mixture can be identified. This can quickly report ee values and is extremely useful in evaluation of the enantiomeric purity and the racemization process of catecholamines. Compared with other chromatography-based separation and detection methods, this method requires no additional derivative modification or separation of enantiomers. It can directly identify catecholamine enantiomers in mixed samples and can be used in the quality control of norepinephrine and epinephrine drug production. Though not demonstrated in this paper, this sensing strategy is, in principle, compatible with other catecholamine enantiomers drugs and metabolites, such as DL-dopa,[41] DL-isoprenaline,[42] and DL-vanillylmandelic acid.[43] The PNRSS strategy may as well be carried out with solid-state nanopores or DNA nanopores in future prospects. Suitable engineering of the PNRSS strand may also inspire other applications of enantiomer sensing.

METHODS

Materials. *Escherichia coli* strain BL21 (DE3) was purchased from Biomed (China). Dioxane-free isopropyl-β-D-thiogalactopyranoside (IPTG), kanamycin sulfate, and tris(hydroxymethyl)aminomethane (Tris) were supplied by Solarbio Biotechnology (China). Luria–Bertani broth and Luria–Bertani agar were from Hopebio (China). Precision Plus Protein Dual Color Standards and TGX FastCast Acrylamide Kit (12%) were purchased from Bio-Rad. D-Epinephrine (98%) was purchased from Shanghai Kewel Chemical Technology Co., Ltd. (China). L-Epinephrine (99%) was purchased from Energy Chemical (China). D-Norepinephrine (98%) was custom synthesized by Nanjing Sunsure Chemical Technology Co., Ltd. (China). L-Norepinephrine (98%), potassium chloride (KCl, 99.9%), sodium hydroxide (NaOH, 99.9%), sodium sulfate anhydrous (Na_2SO_4, 99%), and dimethyl sulfoxide-d_6 (DMSO-d_6, 99.9%D + 0.03%TMS) were from Aladdin (China). 1,2-Diphytanoyl-*sn*-glycero-3-phosphocholine (DPhPC) was purchased from Avanti Polar Lipids. Hexadecane, pentane, ethylenediaminetetraacetic acid (EDTA), and Genapol X-80 were from Sigma-Aldrich. Acetonitrile (MeCN, 99.9%) and methylboronic acid (97%) were supplied by Macklin (China). 4-(2-Hydroxyethyl)-1-piperazine ethanesulfonic acid (HEPES, 99%) was purchased from Shanghai Yuanye Bio-Technology (China). Hydrochloric acid (HCl), acetone (Me_2CO, 99.5%), and dichloromethane (DCM, 99.5%) were purchased from Sinopharm (China). 4-(Azidomethyl)benzeneboronic acid pinacol ester (95%) was from Alfa Aesar (U.S.), and streptavidin was from New England Biolabs.

The monomeric DNA phosphoramidite, 5-ethynyl-dU-CE phosphoramidite, was from Glen Research (U.S.). The alkyne-containing oligonucleotide 14TAK (Supplementary Table 1) was synthesized by Shanghai Generay Biotech Co., Ltd. The sequences of all oligonucleotides are listed in Supplementary Table 1.

Nanopore Preparation. As previously reported,[44] the pet-30a(+) plasmid containing the gene coding for M2MspA (D93N/D91N/D90N/D118R/D134R/E139 K) was custom-synthesized by Genscript (New Jersey, U.S.) and expressed in *E. coli* BL21 (DE3). The produced M2MspA nanopore was purified by nickel affinity chromatography (GE Akta Pure, GE Healthcare) and used for all measurements in this paper. For simplicity, the M2MspA is referred to as MspA throughout this study. The wild type α-hemolysine (WT α-HL) nanopore protein was prepared as previously reported.[44]

Nanopore Measurements and Data Analysis. All nanopore measurements in this study were carried out as previously reported.[33] A self-assembled lipid bilayer consisting of DPhPC separated the measurement device into two chambers. Each chamber contained 500 μL of buffer of 1.5 M KCl, 10 mM HEPES, pH 8.0. A pair of Ag/AgCl electrodes was inserted into two chambers and contacted with buffer. The electrodes were connected with the patch clamp amplifier to form a closed circuit. For convenience, the electrode in *cis* was connected with ground and another electrode in *trans* was the working electrode. Experimentally, with the insertion of single MspA nanopore, the buffer in *cis* was exchanged manually to avoid further pore insertions.

The mean blockage level ($\overline{I_p}$) was acquired from static pore blockage measurements. Briefly, the streptavidin-tethered PNRSS strand was added to *cis* at a concentration of 20 nM, and a voltage protocol of +140 mV (0.9 s) and −100 mV (0.3 s) was repeatedly applied. A minimum of 500 I_p events were collected for each independent measurement. The event histogram results were fitted to a Gaussian distribution, and the central position of the fitting result was $\overline{I_p}$. The results are shown in Supplementary Table 2.

For PNRSS measurements, the streptavidin-tethered PNRSS strand was added to *cis* to reach a 20 nM final concentration, and a +140 mV potential was continually applied. Upon the addition of analytes, continuous blockage events appeared on the basis of I_p and were

https://doi.org/10.1021/acsnano.2c01017
ACS Nano XXXX, XXX, XXX−XXX

recognized as the characteristic events generated by analytes (Supplementary Figure 3).

All electrophysiology measurements were carried out with an Axopatch 200B patch clamp amplifier and digitized by a Digidata 1550B digitizer (Molecular Devices, UK). The traces recorded with the 25 kHz sampling rate and low-pass filtered with a cutoff frequency of 1 kHz. All PNRSS measurements were performed at room temperature (21 ± 2 °C). Nanopore events were extracted by the single channel search function of Clampfit 10.7 (Molecular Devices, U.K.). Further analysis was carried out in Origin 2019. All machine learning algorithms were developed with the Classification Learner toolbox of MATLAB R2019b (MathWorks, U.S.). The custom code and sample data are shared in a public repository (https://github.com/sonic220/Catcholamine-Enantiomer-Classifier/blob/main/Catecholamine%20Enantiomers%20Classifier.zip).

Preparation of the PNRSS Strand 14PBA. The PNRSS strand 14TAK was reacted with 4-(azidomethyl)benzeneboronic acid[33] by a Huisgen copper(I)-catalyzed azide−alkyne 1,3-dipolar cycloaddition (CuAAC) reaction[35] to prepare the PNRSS strand 14PBA, which contained a single PBA. The product 14PBA was characterized by mass spectrometry to confirm the successful conjugation (Supplementary Figure 1). To prepare the streptavidin-tethered DNA complexes, the PNRSS strands 14TAK and 14PBA, which contain a 5′ biotin-TEG modification, were mixed with streptavidin at an equal molar ratio at room temperature for 10 min. The complexes obtained were used for all downstream PNRSS measurements.

ASSOCIATED CONTENT

Supporting Information

The Supporting Information is available free of charge at https://pubs.acs.org/doi/10.1021/acsnano.2c01017.

Supplementary tables: sequence context of all PNRSS strands in this study; statistics of $\overline{I_p}$ for PNRSS strand 14TAK and 14PBA; statistics of the percentage blockade $\overline{\%I_b}$ and t_{off} of catecholamine events; kinetic constants for catecholamine interacting with a PBA: enantiomeric excess values of the mixtures of L- and D-norepinephrine or epinephrine; list of the performance of all machine learning models; Supplementary figures: chemical synthesis and characterization of the PNRSS strand 14PBA; definition of event parameters during PNRSS measurements; independent experiments of D-norepinephrine, L-norepinephrine, D-epinephrine, and L-epinephrine binding to a PBA; discrimination of epinephrine enantiomers with PNRSS; detection of D-norepinephrine and L-epinephrine; features and statistical results of four catecholamine enantiomers events; determination of enantiomeric purity of a mixture of norepinephrine or epinephrine enantiomers; PNRSS detection of epinephrine hydrochloride injection; PNRSS detection of epinephrine enantiomers in urine; PNRSS measurements at low concentration of D-epinephrine; PNRSS detection of epinephrine enantiomers with α-HL nanopore (PDF)

Supplementary movie: PNRSS sensing of norepinephrine and epinephrine enantiomers (MP4)

AUTHOR INFORMATION

Corresponding Author

Shuo Huang − *State Key Laboratory of Analytical Chemistry for Life Sciences, School of Chemistry and Chemical Engineering, Nanjing University, 210023 Nanjing, China; Chemistry and Biomedicine Innovation Center (ChemBIC), Nanjing University, 210023 Nanjing, China;* orcid.org/0000-0001-6133-7027; Email: shuo.huang@nju.edu.cn

Authors

Wendong Jia − *State Key Laboratory of Analytical Chemistry for Life Sciences, School of Chemistry and Chemical Engineering, Nanjing University, 210023 Nanjing, China; Chemistry and Biomedicine Innovation Center (ChemBIC), Nanjing University, 210023 Nanjing, China;* orcid.org/0000-0002-1685-9261

Chengzhen Hu − *State Key Laboratory of Analytical Chemistry for Life Sciences, School of Chemistry and Chemical Engineering, Nanjing University, 210023 Nanjing, China; Chemistry and Biomedicine Innovation Center (ChemBIC), Nanjing University, 210023 Nanjing, China;* orcid.org/0000-0002-6666-418X

Yuqin Wang − *State Key Laboratory of Analytical Chemistry for Life Sciences, School of Chemistry and Chemical Engineering, Nanjing University, 210023 Nanjing, China; Chemistry and Biomedicine Innovation Center (ChemBIC), Nanjing University, 210023 Nanjing, China;* orcid.org/0000-0002-9311-241X

Yao Liu − *State Key Laboratory of Analytical Chemistry for Life Sciences, School of Chemistry and Chemical Engineering, Nanjing University, 210023 Nanjing, China; Chemistry and Biomedicine Innovation Center (ChemBIC), Nanjing University, 210023 Nanjing, China;* orcid.org/0000-0003-3597-2208

Liying Wang − *State Key Laboratory of Analytical Chemistry for Life Sciences, School of Chemistry and Chemical Engineering, Nanjing University, 210023 Nanjing, China; Chemistry and Biomedicine Innovation Center (ChemBIC), Nanjing University, 210023 Nanjing, China;* orcid.org/0000-0002-7226-457X

Shanyu Zhang − *State Key Laboratory of Analytical Chemistry for Life Sciences, School of Chemistry and Chemical Engineering, Nanjing University, 210023 Nanjing, China; Chemistry and Biomedicine Innovation Center (ChemBIC), Nanjing University, 210023 Nanjing, China;* orcid.org/0000-0003-2300-957X

Qiang Zhu − *State Key Laboratory of Analytical Chemistry for Life Sciences, School of Chemistry and Chemical Engineering, Nanjing University, 210023 Nanjing, China*

Yuming Gu − *State Key Laboratory of Analytical Chemistry for Life Sciences, School of Chemistry and Chemical Engineering, Nanjing University, 210023 Nanjing, China*

Panke Zhang − *State Key Laboratory of Analytical Chemistry for Life Sciences, School of Chemistry and Chemical Engineering, Nanjing University, 210023 Nanjing, China;* orcid.org/0000-0001-8562-9972

Jing Ma − *State Key Laboratory of Analytical Chemistry for Life Sciences, School of Chemistry and Chemical Engineering, Nanjing University, 210023 Nanjing, China;* orcid.org/0000-0001-5848-9775

Hong-Yuan Chen − *State Key Laboratory of Analytical Chemistry for Life Sciences, School of Chemistry and Chemical Engineering, Nanjing University, 210023 Nanjing, China*

Complete contact information is available at: https://pubs.acs.org/10.1021/acsnano.2c01017

Author Contributions

S.H. and W.J. conceived the project. W.J. and C.H. performed the measurements. W.J. and Y.L. designed the machine learning algorithms. L.W. and S.Z. prepared the MspA nanopores. Q.Z., Y.G., and J.M. participated in the discussion. P.Z. set up the instruments. S.H. and W.J. wrote the paper. Y.W. and W.J.

https://doi.org/10.1021/acsnano.2c01017
ACS Nano XXXX, XXX, XXX−XXX

prepared the supplementary videos. S.H. and H.-Y.C. supervised the project.

Funding

This project was funded by National Natural Science Foundation of China (Grant Nos. 31972917, 91753108, 21675083, and 22033004), supported by the Fundamental Research Funds for the Central Universities (Grant Nos. 020514380257 and 020514380261), programs for high-level entrepreneurial and innovative talents introduction of Jiangsu Province (individual and group program), Natural Science Foundation of Jiangsu Province (Grant No. BK20200009), Excellent Research Program of Nanjing University (Grant No. ZYJH004), Shanghai Municipal Science and Technology Major Project, State Key Laboratory of Analytical Chemistry for Life Science (Grant No. 5431ZZXM1902), Technology innovation fund program of Nanjing University, and China Postdoctoral Science Foundation (Grant No. 2021M691508).

Notes

The authors declare the following competing financial interest(s): S.H. and W.J. have filed patents describing the PNRSS technology and its applications thereof. The authors claim no other competing interest.

ACKNOWLEDGMENTS

The authors acknowledge Prof. Hagan Bayley (University of Oxford) for valuable suggestions during preparation of the manuscript. The authors acknowledge Prof. Zijian Guo, Prof. Shaolin Zhu, Prof. Congqing Zhu, Prof. Shouyun Yu, Prof. Jin Xie, Prof. Zhuangzhi Shi, Prof. Jie Li and Prof. Ran Xie in Nanjing University for inspiring discussions.

ABBREVIATIONS

MspA, *Mycobacterium smegmatis* porin A; PBA, phenylboronic acid; PNRSS, programmable nanoreactors for stochastic sensing

REFERENCES

(1) Bonner, W. A. The origin and amplification of biomolecular chirality. *Origins Life Evol. Biosphere* **1991**, *21* (2), 59−111.
(2) Bentley, R. Role of sulfur chirality in the chemical processes of biology. *Chem. Soc. Rev.* **2005**, *34* (7), 609−624.
(3) Brand, D. J.; Fisher, J. Molecular structure and chirality. *J. Chem. Educ.* **1987**, *64* (12), 1035−1038.
(4) Ariëns, E. J. Stereochemistry, a basis for sophisticated nonsense in pharmacokinetics and clinical pharmacology. *European Journal of Clinical Pharmacology* **1984**, *26* (6), 663−668.
(5) Lukša, J.; Josič, D.; Kremser, M.; Kopitar, Z.; Milutinovič, S. Pharmacokinetic behaviour of R-(+)- and S-(−)-amlodipine after single enantiomer administration1Presented at the Symposium on New Achievements in Chromatography, Opatija, Croatia, October 8−10, 1996.1. *Journal of Chromatography B: Biomedical Sciences and Applications* **1997**, *703* (1), 185−193.
(6) Agranat, I.; Caner, H.; Caldwell, J. Putting chirality to work: the strategy of chiral switches. *Nat. Rev. Drug Discovery* **2002**, *1* (10), 753−768.
(7) Teo, S. K.; Colburn, W. A.; Tracewell, W. G.; Kook, K. A.; Stirling, D. I.; Jaworsky, M. S.; Scheffler, M. A.; Thomas, S. D.; Laskin, O. L. Clinical Pharmacokinetics of Thalidomide. *Clin. Pharmacokinet.* **2004**, *43* (5), 311−327.
(8) Moore, R. Y.; Bloom, F. E. Central Catecholamine Neuron Systems: Anatomy and Physiology of the Norepinephrine and Epinephrine Systems. *Annu. Rev. Neurosci.* **1979**, *2* (1), 113−168.
(9) Lieberman, P. Use of epinephrine in the treatment of anaphylaxis. *Current Opinion in Allergy and Clinical Immunology* **2003**, *3* (4), 313−318.
(10) Simons, F. E. R. Epinephrine (adrenaline) in the first-aid, out-of-hospital treatment of anaphylaxis. *Novartis Foundation symposium* **2008**, *257*, 228−247.
(11) Patil, P. N.; Li, C.; Kumari, V.; Hieble, J. P. Analysis of efficacy of chiral adrenergic agonists. *Chirality* **2008**, *20* (3−4), 529−543.
(12) Beale, J. M., Jr.; Block, J. H. Adrenergic Agents. *Wilson and Gisvold's Textbook of Organic Medicinal and Pharmaceutical Chemistry*, 12th ed.; Lippincott Williams & Wilkins: Philadelphia, PA, 2011; Vol. *12*, pp 519−557.
(13) Singer, R. A.; Carreira, E. M. An in situ procedure for catalytic, enantioselective acetate aldol addition. Application to the synthesis of (R)-(−)-epinephrine. *Tetrahedron Lett.* **1997**, *38* (6), 927−930.
(14) Fukushima, T.; Murayama, K.; Santa, T.; Homma, H.; Imai, K. Enantiomeric separation of d-/l-norepinephrine and -epinephrine by high-performance liquid chromatography with a β-cyclodextrin type chiral stationary phase. *Biomed. Chromatogr.* **1998**, *12* (1), 1−3.
(15) Zhou, Y.; Dong, J.; Zhang, F.; Gong, Y. Synthesis of C1-Symmetric Chiral Secondary Diamines and Their Applications in the Asymmetric Copper(II)-Catalyzed Henry (Nitroaldol) Reactions. *Journal of Organic Chemistry* **2011**, *76* (2), 588−600.
(16) Xu, Z.; Wu, Q.; Yang, M.; Wang, S.; Wang, Z.; Xu, X. Efficient asymmetric biosynthesis of (R)-(−)-epinephrine in hydrophilic ionic liquid-containing systems. *RSC Adv.* **2016**, *6* (104), 102292−102295.
(17) Gu, G.; Yang, T.; Yu, O.; Qian, H.; Wang, J.; Wen, J.; Dang, L.; Zhang, X. Enantioselective Iridium-Catalyzed Hydrogenation of α-Keto Amides to α-Hydroxy Amides. *Org. Lett.* **2017**, *19* (21), 5920−5923.
(18) Stepensky, D.; Chorny, M.; Dabour, Z.; Schumacher, I. Long-term stability study of L-adrenaline injections: Kinetics of sulfonation and racemization pathways of drug degradation. *J. Pharm. Sci.* **2004**, *93* (4), 969−980.
(19) Lv, H.; Luo, S.; Tian, R.; Zhang, W.; Sun, B.; Cui, Y. Analysis of endogenous epinephrine and norepinephrine enantiomers in rat plasma and application to a stereoselective pharmacokinetics. *J. Pharm. Biomed. Anal.* **2020**, *177*, 112859.
(20) Allgire, J. F.; Juenge, E. C.; Damo, C. P.; Sullivan, G. M.; Kirchhoefer, R. D. High-performance liquid chromatographic determination of d-/l-epinephrine enantiomer ratio in lidocaine-epinephrine local anesthetics. *J. Chromatogr. A* **1985**, *325*, 249−254.
(21) Kirkpatrick, D.; Yang, J.; Trehy, M. Determination of the enantiomeric purity of epinephrine by HPLC with circular dichroism detection. *Journal of Liquid Chromatography & Related Technologies* **2017**, *40* (11), 556−563.
(22) Rosenblum, H.; Goldman, R.; Feldman, H. Determination of the stability of epinephrine by optical rotation*. *Journal of the American Pharmaceutical Association (Scientific ed.)* **1949**, *38* (5), 255−258.
(23) Haque, F.; Li, J.; Wu, H.-C.; Liang, X.-J.; Guo, P. Solid-state and biological nanopore for real-time sensing of single chemical and sequencing of DNA. *Nano Today* **2013**, *8* (1), 56−74.
(24) Cao, J.; Jia, W.; Zhang, J.; Xu, X.; Yan, S.; Wang, Y.; Zhang, P.; Chen, H.-Y.; Huang, S. Giant single molecule chemistry events observed from a tetrachloroaurate(III) embedded Mycobacterium smegmatis porin A nanopore. *Nat. Commun.* **2019**, *10* (1), 5668.
(25) Ramsay, W. J.; Bayley, H. Single-Molecule Determination of the Isomers of D-Glucose and D-Fructose that Bind to Boronic Acids. *Angew. Chem., Int. Ed.* **2018**, *57* (11), 2841−2845.
(26) Venkatesan, B. M.; Bashir, R. Nanopore sensors for nucleic acid analysis. *Nat. Nanotechnol.* **2011**, *6* (10), 615−624.
(27) Yan, S.; Zhang, J.; Wang, Y.; Guo, W.; Zhang, S.; Liu, Y.; Cao, J.; Wang, Y.; Wang, L.; Ma, F.; Zhang, P.; Chen, H.-Y.; Huang, S. Single Molecule Ratcheting Motion of Peptides in a Mycobacterium smegmatis Porin A (MspA) Nanopore. *Nano Lett.* **2021**, *21* (15), 6703−6710.
(28) Liu, Y.; Pan, T.; Wang, K.; Wang, Y.; Yan, S.; Wang, L.; Zhang, S.; Du, X.; Jia, W.; Zhang, P.; Chen, H.-Y.; Huang, S. Allosteric Switching of Calmodulin in a Mycobacterium smegmatis porin A (MspA) Nanopore-Trap. *Angew. Chem., Int. Ed.* **2021**, *60* (44), 23863−23870.
(29) Kang, X.-f.; Cheley, S.; Guan, X.; Bayley, H. Stochastic detection of enantiomers. *J. Am. Chem. Soc.* **2006**, *128* (33), 10684−10685.

https://doi.org/10.1021/acsnano.2c01017
ACS Nano XXXX, XXX, XXX−XXX

(30) Guo, Y.; Niu, A.; Jian, F.; Wang, Y.; Yao, F.; Wei, Y.; Tian, L.; Kang, X. Metal−organic complex-functionalized protein nanopore sensor for aromatic amino acids chiral recognition. *Analyst* **2017**, *142* (7), 1048−1053.
(31) Boersma, A. J.; Bayley, H. Continuous Stochastic Detection of Amino Acid Enantiomers with a Protein Nanopore. *Angew. Chem., Int. Ed.* **2012**, *51* (38), 9606−9609.
(32) Gao, C.; Ding, S.; Tan, Q.; Gu, L.-Q. Method of Creating a Nanopore-Terminated Probe for Single-Molecule Enantiomer Discrimination. *Anal. Chem.* **2009**, *81* (1), 80−86.
(33) Jia, W.; Hu, C.; Wang, Y.; Gu, Y.; Qian, G.; Du, X.; Wang, L.; Liu, Y.; Cao, J.; Zhang, S.; Yan, S.; Zhang, P.; Ma, J.; Chen, H.-Y.; Huang, S. Programmable nano-reactors for stochastic sensing. *Nat. Commun.* **2021**, *12* (1), 5811.
(34) Whyte, G. F.; Vilar, R.; Woscholski, R. Molecular recognition with boronic acids—applications in chemical biology. *J. Chem. Biol.* **2013**, *6* (4), 161−174.
(35) Kolb, H. C.; Finn, M. G.; Sharpless, K. B. Click Chemistry: Diverse Chemical Function from a Few Good Reactions. *Angew. Chem., Int. Ed.* **2001**, *40* (11), 2004−2021.
(36) Butler, T. Z.; Pavlenok, M.; Derrington, I. M.; Niederweis, M.; Gundlach, J. H. Single-molecule DNA detection with an engineered MspA protein nanopore. *P Natl. Acad. Sci. USA* **2008**, *105* (52), 20647−20652.
(37) Wang, Y.; Guan, X.; Zhang, S.; Liu, Y.; Wang, S.; Fan, P.; Du, X.; Yan, S.; Zhang, P.; Chen, H.-Y.; Li, W.; Zhang, D.; Huang, S. Structural-profiling of low molecular weight RNAs by nanopore trapping/translocation using Mycobacterium smegmatis porin A. *Nat. Commun.* **2021**, *12* (1), 3368.
(38) Wei, Z.-X.; Ying, Y.-L.; Li, M.-Y.; Yang, J.; Zhou, J.-L.; Wang, H.-F.; Yan, B.-Y.; Long, Y.-T. Learning Shapelets for Improving Single-Molecule Nanopore Sensing. *Anal. Chem.* **2019**, *91* (15), 10033−10039.
(39) Cardozo, N.; Zhang, K.; Doroschak, K.; Nguyen, A.; Siddiqui, Z.; Bogard, N.; Strauss, K.; Ceze, L.; Nivala, J. Multiplexed direct detection of barcoded protein reporters on a nanopore array. *Nat. Biotechnol.* **2022**, *40* (1), 42−46.
(40) Finn, M. G. Emerging methods for the rapid determination of enantiomeric excess. *Chirality* **2002**, *14* (7), 534−540.
(41) Misu, Y.; Goshima, Y.; Miyamae, T. Is DOPA a neurotransmitter? *Trends Pharmacol. Sci.* **2002**, *23* (6), 262−268.
(42) Nichtova, Z.; Novotova, M.; Kralova, E.; Stankovicova, T. Morphological and functional characteristics of models of experimental myocardial injury induced by isoproterenol. *General Physiology and Biophysics* **2012**, *31* (2), 141−151.
(43) Blanco-López, M. C.; Lobo-Castañón, M. J.; Miranda-Ordieres, A. J.; Tuñón-Blanco, P. Voltammetric sensor for vanillylmandelic acid based on molecularly imprinted polymer-modified electrodes. *Biosens. Bioelectron.* **2003**, *18* (4), 353−362.
(44) Wang, Y.; Yan, S.; Zhang, P.; Zeng, Z.; Zhao, D.; Wang, J.; Chen, H.; Huang, S. Osmosis-Driven Motion-Type Modulation of Biological Nanopores for Parallel Optical Nucleic Acid Sensing. *ACS Appl. Mater. Interfaces* **2018**, *10* (9), 7788−7797.

https://doi.org/10.1021/acsnano.2c01017
ACS Nano XXXX, XXX, XXX−XXX